

Persistent magnetization at neutrino pair emission

M. Yoshimura

Research Institute for Interdisciplinary Science, Okayama University
Tsushima-naka 3-1-1 Kita-ku Okayama 700-8530 Japan

arXiv:2004.03812v1 [hep-ph] 8 Apr 2020

ABSTRACT

Measurement of parity violating magnetization is proposed as a means to determine neutrino properties such as Majorana/Dirac distinction and absolute neutrino masses. The process we use is radiative neutrino pair emission from a collective and coherent body of lanthanoid ions doped in host crystals. A vector-component of electron spin flip parallel to photon direction emitted from ion excited state generates this type of magnetization which is stored for a long time in crystals till spin relaxation time.

Keywords Majorana neutrino, neutrino mass, parity violation, neutrino pair emission, magnetization of lanthanoid ions, SQUID

1 Introduction

Measurement of parity odd quantity in radiative neutrino pair emission (RENP) [1] is of great use to distinguish the process involving weak interaction from purely QED processes [2]. An interesting quantity of this nature is magnetization parallel to the emitted photon direction along with neutrino pair emission: expectation value in the final state $|f\rangle$, $2\mu_B\langle f|\hat{k}\cdot\vec{S}|f\rangle$, where \hat{k} is the unit vector along the emitted photon momentum and \vec{S} is the electron spin operator with μ_B the Bohr magneton. This quantity is parity odd and time reversal (T) even. The generated magnetization persists till spin relaxation time.

Parity odd quantity may emerge from interference term of parity even and odd operators in the weak hamiltonian H_W of neutrino pair emission. Writing the neutrino pair emission hamiltonian in terms of the neutrino mixing matrix elements, U_{ei} , $i = 1, 2, 3$, $\nu_e = \sum_i U_{ei}\nu_i$, the hamiltonian is given by

$$H_W = \frac{G_F}{\sqrt{2}} \sum_{ij} \bar{\nu}_i \gamma^\alpha (1 - \gamma_5) \nu_j \bar{e} (\gamma_\alpha c_{ij} - \gamma_\alpha \gamma_5 b_{ij}) e \equiv \frac{G_F}{\sqrt{2}} (\mathcal{N}_c^\alpha \bar{e} \gamma_\alpha e - \mathcal{N}_c^\alpha \bar{e} \gamma_\alpha \gamma_5 e), \quad (1)$$

$$b_{ij} = U_{ei}^* U_{ej} - \frac{1}{2} \delta_{ij}, \quad c_{ij} = U_{ei}^* U_{ej} - \frac{1}{2} (1 - 4 \sin^2 \theta_w) \delta_{ij} = b_{ij} + 2 \sin^2 \theta_w \delta_{ij}, \quad (2)$$

where ν_i denotes a neutrino mass eigenstate of mass m_i . The dominant interference term of parity violation arises from product of spatial part of axial vector current of electron, the spin operator $\bar{e} \vec{\gamma} \gamma_5 e \sim \langle \vec{S} \rangle$ (in the non-relativistic limit), and spatial part of vector current, the velocity operator $\bar{e} \vec{\gamma} e \sim \langle \vec{v} \rangle = \langle \vec{p} / m_e \rangle$. Roughly, magnetization caused by (ij) neutrino-pair emission is proportional to $\Re(b_{ij} c_{ij})$, assuming CP conservation, while RENP event rate is proportional to $\Re(b_{ij}^2)$. Experimentally, the weak mixing angle is given by $1 - 4 \sin^2 \theta_w \sim 0.046 \pm 0.0064$. Matrix elements of spin $\langle \vec{S} \rangle$ and velocity operator $\langle \vec{v} \rangle$ are usually of order unity vs a number less than 10^{-3} , hence interference terms are at least smaller by 10^{-3} than rate, a parity even quantity. We shall quantify this ratio for lanthanoid ion we use as target.

Using an effective hamiltonian H'_W of RENP, one calculates generated magnetization,

$$\sum_{\nu} \langle f | \hat{k} \cdot \vec{S} | f \rangle |\langle f | H'_W | e \rangle|^2 = \sum_{\nu} \langle e | H'_W | f \rangle \langle f | \hat{k} \cdot \vec{S} | f \rangle \langle f | H'_W | e \rangle, \quad (3)$$

where neutrino variables, their helicities and momenta, are summed over. Hamiltonian H_W , hence H'_W as well, contains both parity even and parity odd operators due to weak interaction of neutrino pair emission. One of hamiltonian matrix elements in eq.(3) must be parity even and the other parity odd, requiring interference of these. Furthermore, in order to have a non-vanishing $\langle f | \hat{k} \cdot \vec{S} | f \rangle$, the state $|f\rangle$, an energy eigenstate of unperturbed parity even hamiltonian H_0 , must contain both parity even and odd components. This peculiar situation, which never occurs in isolated atoms, arises when ions are placed in crystals, since crystal field acting on target ions provides parity mixing. In other words, host crystals provide environmental parity violation. Lanthanoid ions of $4f^n$ ($n = 11$ for Er^{3+}) system gives rise to what is called forced electric dipole, as pointed out in [3] and its calculation method formulated in [4]. This is why we adopt lanthanoid ions doped in host crystals as targets. Moreover, 4f electrons in lanthanoid ions are insensitive to environment of host crystals due to filled 5s and 5p electrons in outer shells, which give large spin relaxation time, very important to magnetization measurement. Lanthanoid ions doped with low concentration exhibit paramagnetic property at room temperature.

There have been two proposed methods that use a collective and coherent body of atoms to study still unknown neutrino properties [1], [5]. The method we propose here is different from previous proposals in that we detect accumulated effect remaining in target medium rather than measuring individual events themselves. If the accumulated magnetization is above the sensitivity level of detectors, for instance, a high quality SQUID, then the method is found to be very sensitive to Majorana/Dirac distinction, as shown below. Our approach does not assume the nature of neutrino masses, but lanthanoid experiments can determine whether neutrinos are of Majorana or of Dirac type by measuring angular distribution of magnetization caused by interference terms intrinsic to Majorana neutrino, but absent in the Dirac neutrino case [6]. Measurement of smallest neutrino mass at several meV level in three flavor scheme requires high statistics

data, or use of smaller Stark level transitions in crystals. Since there exist a rich variety of J-manifold levels in some lanthanoid ions, both measurement of Majorana/Dirac distinction and smallest neutrino mass seems possible.

Process without photon emission $|e\rangle \rightarrow |g\rangle + \nu\bar{\nu}$ might be considered for magnetization measurement, but estimate gives rate much smaller than detection level. Radiative neutrino pair emission $|e\rangle \rightarrow |g\rangle + \gamma + \nu\bar{\nu}$ [1] gives 10 orders of magnitude larger rates than the process without photon emission. Raman stimulated radiative emission $\gamma + |e\rangle \rightarrow |g\rangle + \gamma + \nu\bar{\nu}$ [5] is also conceivable [7], but the present scheme is simpler and has a better sensitivity to neutrino properties.

We use the natural unit of $\hbar = c = 1$ throughout the present work unless otherwise stated.

2 Magnetization generated at RENP (Radiative Emission of Neutrino Pair)

RENP de-excitation path of ion states is defined as $|e\rangle \rightarrow |p\rangle \rightarrow |g\rangle$ with energies $\epsilon_e > \epsilon_p > \epsilon_g$. This is a cascade process in which neutrino pair is emitted at $|e\rangle \rightarrow |p\rangle$ followed by stimulated photon emission at $|p\rangle \rightarrow |g\rangle$: $|e\rangle \rightarrow |g\rangle + \gamma_0 + \nu\bar{\nu}$.

Probability amplitude of RENP including parity violating terms is given by

$$\mathcal{M} = \frac{G_F}{\sqrt{2}} \frac{\vec{\mu}_{pg} \cdot \vec{B}_0}{\omega_0 - \epsilon_{pg} + i\gamma_p/2} (\vec{S}_{ep} \cdot \vec{N}_b + \frac{\vec{p}_{ep}}{m_e} \cdot \vec{N}_c), \quad (4)$$

where $\vec{N}_{b,c}$ is the neutrino pair emission current defined by eq.(1). Magnetic dipole transition given by $\vec{\mu}_{pg} \cdot \vec{B}_0$ in this formula is usually dominant for $4f^n$ lanthanoid optical transitions among ion lower levels, where \vec{B}_0 is RENP trigger field strength with its frequency given by ω_0 . There may be a forced electric dipole transition of the form, $\vec{e}_{pg} \cdot \vec{E}_0$, as well in lanthanoid ion transitions. To maximize RENP rates, we irradiate the trigger beam at resonant frequency, $\omega_0 = \epsilon_{pg}$, equated to a level energy spacing. Convolution integral of squared resonance function $\propto 1/((\omega_0 - \epsilon_{pg})^2 + \gamma_p^2/4)$ with the Lorentzian spectrum gives $4/(\Delta\omega_0\gamma_p)$, hence we use, in rate formulas below, the laser peak power $P_0 = \vec{B}_0^2 = \vec{E}_0^2$ and its (angular) frequency width $\Delta\omega_0 = 2\pi\Delta\nu_0$. The width factor γ_p in the resonance formula is equal to $\text{Max}(\Delta\omega_0, \text{inverse lifetime of state } |p\rangle \text{ or } |e\rangle)$.

We fully exploit macro-coherent amplification mechanism [1] to enhance rates of weak processes. The macro-coherence amplification has been experimentally verified in weak QED processes of two-photon emission of para-hydrogen vibrational transitions [8]. Compared with spontaneous emission rate, the amplification factor was $\sim 10^{18}$ in these experiments. Rates of macro-coherent amplification are in proportion to $n^2V = nN$ where n is the number density of target atoms and V is the volume of target region with N the number of total target atoms. Macro-coherent rates are thus enhanced by n in contrast to spontaneous emission rate $\propto N$. When macro-coherence works, both the energy and the momentum conservation holds (neglecting very small atomic recoil), to give rates given by a phase-space integrated quantity of

$$|\mathcal{M}|^2 n^2 V (2\pi)^4 \delta^{(4)}(p_e - p_g - k_0). \quad (5)$$

The phase-space integrated RENP rates are given by

$$\Gamma_{\text{RENP1}} = \frac{G_F^2}{24\pi} \frac{P_0}{\Delta\nu_0} \frac{\gamma_{pg}}{\epsilon_{pg}^3 \gamma_p} |\rho_{eg}|^2 |\vec{S}_{ep}|^2 n^2 V \mathcal{F}, \quad \mathcal{F} = \sum_{ij} \mathcal{F}_{ij} \Theta(\mathcal{M}^2 - (m_i + m_j)^2), \quad (6)$$

$$4\pi \mathcal{F}_{ij} = \left\{ \left(1 - \frac{(m_i + m_j)^2}{\mathcal{M}^2}\right) \left(1 - \frac{(m_i - m_j)^2}{\mathcal{M}^2}\right) \right\}^{1/2} [|b_{ij}|^2 (\mathcal{M}^2 - m_i^2 - m_j^2) - 2\delta_M \Re(b_{ij}^2) m_i m_j], \quad (7)$$

$$\mathcal{M}^2 = (\epsilon_{eg} - \omega_0)^2 - (\vec{p}_{eg} - \vec{k}_0)^2 = (1 - r^2)\epsilon_{eg}^2 - 2\epsilon_{eg}\epsilon_{pg}(1 - r \cos \theta) \equiv \mathcal{M}^2(\theta), \quad (8)$$

for parity conserving part, and

$$\Gamma_{\text{RENP2}} = \frac{G_F^2 P_0}{12\pi \Delta\nu_0} \frac{\gamma_{pg}}{\epsilon_{pg}^3 \gamma_p} |\rho_{eg}|^2 \vec{S}_{ep} \cdot \frac{\vec{p}_{ep}}{m_e} n^2 V \mathcal{G}, \quad \mathcal{G} = \sum_{ij} \mathcal{G}_{ij} \Theta(\mathcal{M}^2 - (m_i + m_j)^2), \quad (9)$$

$$4\pi \mathcal{G}_{ij} = \left\{ \left(1 - \frac{(m_i + m_j)^2}{\mathcal{M}^2}\right) \left(1 - \frac{(m_i - m_j)^2}{\mathcal{M}^2}\right) \right\}^{1/2} [\Re(c_{ij}^* b_{ij}) (\mathcal{M}^2 - m_i^2 - m_j^2) - 2\delta_M \Re(c_{ij} b_{ij}) m_i m_j], \quad (10)$$

for parity violating part. Majorana/Dirac difference appears in terms $\propto \delta_M$: $\delta_M = 1$ for Majorana neutrino due to the effect of anti-symmetrized wave functions of two identical fermions [6], and $= 0$ for Dirac neutrino. We neglected small contribution in Γ_{RENP1} from squared vector current $\propto (\vec{p}_{pe}/m_e)^2$.

The mass squared function $\mathcal{M}^2(\theta)$ is invariant mass squared given to neutrino pairs and a function of measurable quantity θ . The same function determines six neutrino-pair emission thresholds at different directions θ given by $\mathcal{M}^2(\theta) = (m_i + m_j)^2$, $i, j = 1, 2, 3$. It also plays important roles in QED background rejection, as discussed below. The initial spatial phase vector \vec{p}_{eg} given at excitation was parametrized by $|\vec{p}_{eg}| = r\epsilon_{eg}$ with its direction θ away from the RENP trigger beam.

We adopt for excitation scheme two-photon cascade process using two pulsed lasers: $\gamma_1 + |g\rangle^\pm \rightarrow |q\rangle^\mp$ and $\gamma_2 + |q\rangle^\mp \rightarrow |e\rangle^\pm$. This way two relevant states, $|g\rangle$ and $|e\rangle$, have the same time reversal quantum numbers, $T = \pm$, since single photon process is governed by time reversal odd operator whether it is of magnetic dipole or electric dipole. Counter-propagating two-photon cascade excitation requires frequencies of two lasers to satisfy $\omega_1 + \omega_2 = \epsilon_{eg}$, $\omega_1 - \omega_2 = r\epsilon_{eg}$. A maximal excitation rate is provided when two frequencies ω_i are matched to level spacings, namely resonant excitation. The neutrino-pair emission operator is also T-odd. T-even two-photon excitation here helps to reject QED background processes, as discussed later.

The quantity ρ_{eg} (called coherence in the optics literature) that appears in rate formulas, eq.(6) and eq.(9), is generated at excitation to $|e\rangle$, its maximum value being 1/2. It is in general time dependent, too. Estimate of this quantity requires detailed simulations of Maxwell-Bloch equations, a set of non-linear partial differential equations that deal with ion state wave functions and propagating electromagnetic fields in a simplified spacetime of one space and one time dimensions [1]. In a off-resonance Raman excitation simulations suggest that this quantity is of order 10^{-3} or less. We expect a larger coherence of order $10^{-1} \sim 10^{-2}$ in the on-resonance cascade excitation adopted here.

Magnetization is a macroscopic quantity given by

$$2\mu_{\text{eff}} n \approx 6.6 \text{ G} \frac{n}{10^{18} \text{ cm}^{-3}} \text{ (for Er}^{3+}\text{)}, \quad (11)$$

using $\mu_{\text{eff}} = g\sqrt{J(J+1)} \approx 9.5\mu_B$ for Er^{3+} in its ground state as an illustration. The generated magnetization by RENP is this value times interference rate, Γ_{RENP2} of eq.(9).

Both rates $\propto \mathcal{F}$ and magnetization $\propto \mathcal{G}$ are functions of the mass squared function $\mathcal{M}^2(\theta)$. In measuring the angular distribution of signals one may use a single trigger beam at different directions of irradiation to determine neutrino-pair thresholds. Six thresholds have different weights, which are calculable from neutrino oscillation data [9] and listed in the following table, assuming CP conservation case described by real number b_{ij}, c_{ij} .

	(11)	(12)	(22)	(13)	(23)	(33)
rate	0.0311	0.405	0.0401	0.0325	0.0144	0.227
magnetization	0.508	0.405	0.517	0.0325	0.0144	0.704

Spin factors are calculated as follows. We consider unpolarized targets, hence average over initial $|e\rangle$ magnetic quantum numbers and sum over final $|p\rangle$ magnetic quantum numbers. Using Wigner-Eckart theorem applied to manifolds of the same J value (in actual application $J = 11/2$), one may relate \vec{S}_{ep}^2

and $\vec{S}_{ep} \cdot \vec{p}_{ep}/m_e$ to electric and magnetic dipole transition rates. Summation and average over magnetic J quantum numbers of two state gives $(\vec{S}_{ep} \cdot \vec{p}_{ep}/m_e)^2 = \vec{S}_{ep}^2 (\vec{p}_{ep}/m_e)^2$. Relation of spin and velocity matrix elements to transition rates is $\gamma_{ep}^E = e^2 (\vec{p}_{ep}/m_e)^2 \Delta_{ep}/3\pi$ and $\gamma_{ep}^M = \vec{S}_{ep}^2 \mu_{ep}^2 \Delta_{ep}^3/3\pi$ where Δ_{ep} is the energy difference of two states. Hence $(\vec{p}_{ep}/m_e)^2/\vec{S}_{ep}^2 = e^2/(\mu_{ep}^2 \Delta_{ep}^2) = (2m_e/g\Delta_{ep})^2$ with the Lande g-factor $g = 2$ of electron spin. This gives

$$\frac{|\vec{v}_{ep}|}{|\vec{S}_{ep}|} = \frac{\Delta_{ep}}{m_e} \sqrt{\frac{\gamma_{ep}^E}{\gamma_{ep}^M}} \equiv \left(\frac{v}{S}\right)_{ep}. \quad (12)$$

We illustrate an example of v/S calculations for Er^{3+} in Appendix. For unpolarized targets \vec{S}_{ep}^2 is of order unity, close to $(2J_p + 1)/(2J_e + 1)$.

To obtain a large PV/PC ratio it is desirable to use a large electric/magnetic transition ratio, since the ratio $\frac{\Delta_{pe}}{m_e} \approx 10^{-6}$ is small. In lanthanoid ions doped in crystals transitions among low lying levels are predominantly magnetic, and it is desirable to have a large forced electric dipole transition. For trivalent Kramers ions such as Er^{3+} placed at a less symmetric cite (not inversion center for instance) are necessary. Even in cubic crystals trivalent lanthanoid ions often substitute at sites of less symmetry, C_2 site instead of C_{3i} IC (Inversion Center). In this respect trivalent Er ion doped in host crystal such as YSO may give larger magnetization than the example here.

3 Dominant QED background

It is easy to understand that both of macro-coherently amplified QED events, $|e\rangle^\pm \rightarrow |g\rangle^\pm + \gamma\gamma$ and $|e\rangle^\pm \rightarrow |g\rangle^\mp + \gamma$ do not exist by kinematic choice of a positive mass squared function $\mathcal{M}^2(\theta)$, which constrains trigger directions θ for a specified chosen parameter r . Major backgrounds appear to be macro-coherently amplified $|e\rangle^\pm \rightarrow |g\rangle^\mp + \gamma\gamma\gamma$ (called McQ3) and spontaneous emission of a single photon. McQ3 events are however characterized by a time reversal odd transition, which is distinguished from time reversal even RENP process, $|e\rangle^\pm \rightarrow |g\rangle^\pm + \gamma + \nu\bar{\nu}$. This way one can kill time reversal odd transition McQ3 and spontaneous single photon emission, leaving McQ4 $|e\rangle^\pm \rightarrow |g\rangle^\pm + \gamma\gamma\gamma\gamma$ the major QED background.

McQ4 do not contribute to magnetization. The only thing one has to worry about is depletion of prepared state $|e\rangle^\pm$. A crude estimate of McQ4 event rate shows that it is a few to several orders of magnitudes larger than RENP rate. With extra emitted photon detection, this remaining background is presumably controllable even in rate measurements.

4 Example of Er^{3+} RENP scheme

Trivalent Er ion has a rich J-manifold structure, as illustrated in Appendix. The ion is at inversion center of this crystal, but J-manifold structure is insensitive to crystal environments. We consider the following de-excitation path of time reversal degeneracy:

$$|e\rangle = {}^4\text{H}_{11/2}^\pm(2.3946) \rightarrow {}^4\text{I}_{11/2}^\mp|g\rangle = {}^4\text{I}_{15/2}^\pm(0), \quad (13)$$

and cascade excitation of frequencies,

$$\omega_1 = 1.5894\text{eV}(= \epsilon({}^4\text{H}_{11/2} - {}^4\text{I}_{13/2})), \quad \omega_2 = 0.805\text{eV}(= \epsilon({}^4\text{I}_{13/2} - {}^4\text{I}_{15/2})), \quad r = 0.3276. \quad (14)$$

J-manifolds are split by crystal field, giving Stark levels having two-fold Kramers degeneracy. We ignore effects of different Stark levels for simplicity. In order to maintain the doubled rate of time reversal degeneracy, it is necessary to shield earth magnetic field.

Using Er^{3+} data given in Appendix, we estimate RENP rate Γ and generated magnetization M :

$$\Gamma = 1.3 \times 10^{-3} \text{sec}^{-1} \frac{\mathcal{F}}{\text{eV}^2} |\rho_{eg}|^2 |\vec{S}_{ep}|^2 \left(\frac{n}{10^{18} \text{cm}^{-3}}\right)^2 \frac{V}{10^{-2} \text{cm}^3} \frac{P_0}{\text{GWcm}^{-2}} \frac{100 \text{MHz}}{\Delta\nu_0}, \quad (15)$$

$$M = 7.3 \times 10^{-9} \text{G sec}^{-1} \frac{\mathcal{G}}{\text{eV}^2} |\rho_{eg}|^2 |\vec{S}_{ep}|^2 \left(\frac{n}{10^{18} \text{cm}^{-3}}\right)^3 \frac{V}{10^{-2} \text{cm}^3} \frac{P_0}{\text{GWcm}^{-2}} \frac{100 \text{MHz}}{\Delta\nu_0}. \quad (16)$$

For this estimate we used numbers appropriate for pulsed trigger laser. For (continuous wave) CW operation $P_0 = 1 \text{kWcm}^{-2}$, $\Delta\nu_0 = 1 \text{kHz}$, hence 1/10 reductions of rate and magnetization are more appropriate for CW.

Magnetization calculated this way is measurable, being comparable to, or above, the SQUID sensitivity level used in fundamental physics experiments such as in axion force experiments, [11], [12], [13] and axion haloscope experiment [14], [15].

We show magnetization curves, its angular θ distributions at a specific excitation parameter r , in Fig(1) and Fig(2). For comparison rate angular distribution is shown in Fig(3). Magnetization depends on $b_{ij} \times c_{ij}$ above (ij) pair thresholds, while rate depends on b_{ij}^2 . This difference, as numerically shown in the table, explains a high sensitivity of magnetization to the Majorana/Dirac distinction. On the other hand, it is difficult to distinguish mass types from rate, as seen in Fig(3). Absolute mass determination is harder, and one needs a high statistics data near the end point of angular distribution, as shown in Fig(2).

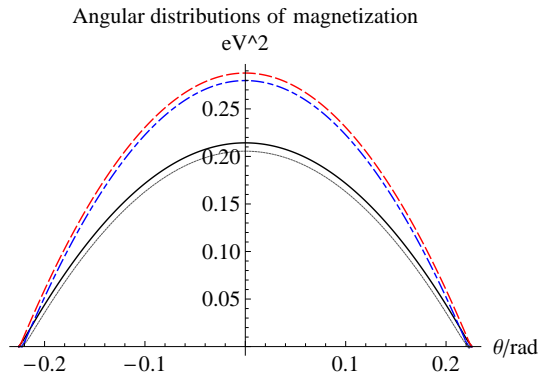


Figure 1: Angular θ distribution of magnetization given by $4\pi\mathcal{G}(\theta)$ for $r = 0.3276$: NH (Normal Hierarchy) Majorana neutrinos of smallest mass 5 meV in solid black, 50 meV in dotted black, NH Dirac 5 meV in dashed red, and 50 meV in dash-dotted blue. All CP violating phases are assumed to vanish for simplicity. Absolute values of magnetization are obtained by multiplying numbers here with $7.3 \times 10^{-9} \text{G sec}^{-1}$ of eq.(16).

5 Towards Er^{3+} experimental design

There are many works to be done before we prepare technical design report of actual experiments.

First, results in the present work are incomplete in several places:

- (1) Lack of theoretical calculations or experimental results of crystal field effect in a variety of host crystals, namely, Stark levels and forced electric dipole transition rates along with magnetic transition among low lying levels for trivalent Er ions.
- (2) Simulation estimate of the coherence $\rho_{eg}(t)$ assuming excitation scheme and laser specification.
- (3) Simulation of McQ4 QED backgrounds in order to identify and isolate background events.
- (4) Design of SQUID detection system.

Experimental R and D studies are even more important. One may list some items:

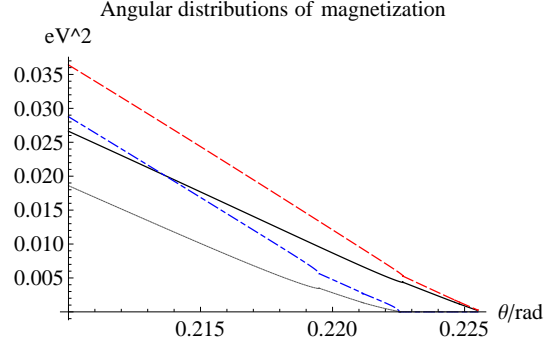


Figure 2: Enlarged end point region corresponding to Fig(1).

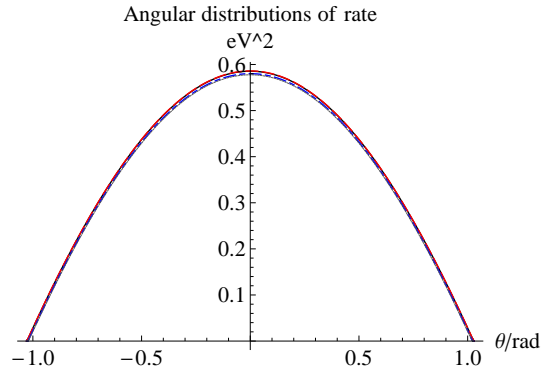


Figure 3: Angular θ distribution of rate given by $4\pi\mathcal{F}(\theta)$ for $r = 0.3276$: NH Majorana of smallest mass 5 meV in solid black, 50 meV in dotted black, NH Dirac 5 meV in dashed red, and 50 meV in dash-dotted blue. All CP violating phases are assumed to vanish for simplicity. Absolute values of rate are obtained by multiplying numbers here with $1.3 \times 10^{-3} \text{ sec}^{-1}$ of eq.(15).

- (5) Optical measurements of $4f^{11}$ manifolds in candidate host crystals.
(6) Study of relaxation processes, in particular, phonon related relaxation at low temperatures.

6 Appendix: Er^{3+} data and estimated parity violating component

We consider a special host crystal, $\text{Er}^{3+}:\text{Cs}_2\text{NaYF}_6$ or $:\text{Y}_2\text{O}_3$ for concreteness. Trivalent Er ion substitutes inversion center of Y. According to [10], calculated radiative decay rates of 10% doped Er^{3+} in host Cs_2NaYF_6 are

initial	final	energy/eV	rate/sec ⁻¹	radiative life/msec	$v/S(10^{-6})$
${}^4\text{I}_{13/2} \rightarrow$	${}^4\text{I}_{15/2}$	0.805	$24.82^{\text{MD}} + 2.46^{\text{ED}}$	36.7	0.25
${}^4\text{I}_{11/2} \rightarrow$	${}^4\text{I}_{15/2}$	1.286	4.13^{ED}	113.4	
	${}^4\text{I}_{13/2}$	0.481	$4.26^{\text{MD}} + 0.42^{\text{ED}}$		0.15
${}^4\text{I}_{9/2} \rightarrow$	${}^4\text{I}_{15/2}$	1.563	9.46^{ED}	73.3	
	${}^4\text{I}_{13/2}$	0.7575	3.48^{ED}		
	${}^4\text{I}_{11/2}$	0.277	$0.67^{\text{MD}} + 0.02^{\text{ED}}$		0.047
${}^4\text{F}_{9/2} \rightarrow$	${}^4\text{I}_{15/2}$	1.9014	58.91^{ED}	14.6	
	${}^4\text{I}_{13/2}$	1.0964	3.5^{ED}		
	${}^4\text{I}_{11/2}$	0.619	$3.49^{\text{MD}} + 1.06^{\text{ED}}$		0.33
	${}^4\text{I}_{9/2}$	0.339	$1.34^{\text{MD}} + 0.18^{\text{ED}}$		0.12
${}^4\text{S}_{3/2} \rightarrow$	${}^4\text{I}_{15/2}$	2.2645eV	4.93^{ED}	131.6	
	${}^4\text{I}_{13/2}$	1.4593eV	2.02^{ED}		
	${}^4\text{I}_{11/2}$	0.9785eV	0.18^{ED}		
	${}^4\text{I}_{9/2}$	0.7017eV	0.48^{ED}		
${}^4\text{H}_{11/2} \rightarrow$	${}^4\text{I}_{15/2}$	2.3946eV	518.02^{ED}	1.7	
	${}^4\text{I}_{13/2}$	1.5894eV	$49.43^{\text{MD}} + 7.91^{\text{ED}}$		0.62
	${}^4\text{I}_{11/2}$	1.1091eV	$5.58^{\text{MD}} + 4.73^{\text{ED}}$		1.0
	${}^4\text{I}_{9/2}$	0.8318eV	$0.49^{\text{MD}} + 5.52^{\text{ED}}$		2.7

Low lying levels of Er^{3+} have configuration $4f^{11}$ and its ground state ${}^4\text{I}_{15/2}$ has the effective magnetic moment related to the Lande factor $\mu_{\text{eff}} = g\sqrt{J(J+1)} = 9.5$ (experimental value). Ratio of parity violating to conserving amplitude given by v/S was estimated by using the formula in the text. Low values of v/S here are presumably related to Er^{3+} site at inversion center (IC) of host crystals. Without IC v/S 's are expected to be larger.

Acknowledgements

This research was partially supported by Grant-in-Aid 17H02895 from the Ministry of Education, Culture, Sports, Science, and Technology.

References

- [1] A. Fukumi et al., Prog. Theor. Exp. Phys. (2012) 04D002.
[2] M. Yoshimura, N. Sasao, and S. Uetake, Phys.Rev.D **90**, 013022 (2014).
[3] J.H. Van Vleck, J. Chem. Phys. **41**, 67 (1937).
[4] B.R. Judd, Phys.Rev.**127**, 750(1962). G.S. Ofelt, J. Chem. Phys. **37**, 511 (1961).

- [5] H. Hara and M. Yoshimura, Eur.Phys.J. **C79** 684(2019), and arXiv: 1904.03813v1 (2019).
- [6] M. Yoshimura, Phys. Rev. **D75**, 113007(2007).
- [7] Scheme presented at the talk in workshop on " Determination of the effective electron neutrino mass" at ECT*, Trento, Italy, February 11 (2020).
- [8] Y. Miyamoto et al., PTEP, 113C01 (2014). Y. Miyamoto et al., PTEP, 081C01 (2015). T. Hiraki et al., J. Phys. B: At. Mol. Opt. Phys. **52** 045401 (2019).
- [9] For a review of neutrino oscillation experiments, Particle Data Group Collaboration, M. Tanabashi et al., Phys. Rev. D 98 030001 (2018).
- [10] P.A. Loiko et al., J. Luminescence, **185** , 279 (2017).
- [11] N. Crescini, C. Braggio, G. Carugno,, P. Falferi,, A. Ortolan, and G. Ruoso, Phys.Lett. **B773**, 677 (2017).
- [12] W.-T. Ni, S.-s. Pan, H.-C. Yeh, L.-S. Hou, J. Wan, Phys. Rev. Lett. **82**, 2439 (1999).
- [13] J.E. Moody and F. Wilczek, Phys. Rev. **D30**, 130 (1984).
- [14] S.J. Asztalos et al, Nucl. Inst. and Methods, **A656**, 39 (2011).
T. Braine et al., Phys.Rev.Lett. **124**, 101303 (2020).
The quoted lowest microwave power measurable in ADMX experiment is 2.2×10^{-23} W, which corresponds to event rate $\sim 1 \times 10^{-4}\text{sec}^{-1}$ for 1 eV energy emission.
- [15] P. Sikivie, Phys.Rev.Lett. **51**, 1415 (1983).